Motion-Compensated Defect Interpolation for Flat-Panel Detectors

Til Aach[a], Erhardt Barth[b], Claudia Mayntz[a]

[a]Institute for Signal Processing, University of Lübeck
Ratzeburger Allee 160 D-23538 Lübeck, Germany
[b] Institute for Neuro- and Bioinformatics, University of Lübeck
Ratzeburger Allee 160 D-23538 Lübeck, Germany

ABSTRACT

One advantage of flat-panel X-ray detectors is the immediate availability of the acquired images for display. Current limitations in large-area active-matrix manufacturing technology, however, require that the images read out from such detectors be processed to correct for inactive pixels. In static radiographs, these defects can only be interpolated by spatial filtering. Moving X-ray image modalities, such as fluoroscopy or cine-angiography, permit to use temporal information as well. This paper describes interframe defect interpolation algorithms based on motion compensation and filtering. Assuming the locations of the defects to be known, we fill in the defective areas from past frames, where the missing information was visible due to motion. The motion estimator is based on regularized block matching, with speedup obtained by successive elimination and related measures. To avoid the motion estimator locking on to static defects, these are cut out of each block during matching. Once motion is estimated, three methods are available for defect interpolation: direct filling-in by the motion-compensated predecessor, filling-in by a 3D-multilevel median filtered value, and spatiotemporal mean filtering. Results are shown for noisy fluoroscopy sequences acquired in clinical routine with varying amounts of motion and simulated defects up to six lines wide. They show that the 3D-multilevel median filter appears as the method of choice since it causes the least blur of the interpolated data, is robust with respect to motion estimation errors and works even in non-moving areas.

Keywords: flat panel X-ray detectors, X-ray fluoroscopy, X-ray angiography, inactive pixels, motion estimation, motion compensation, defect replenishment, multilevel median filtering.

1. INTRODUCTION

Flat-panel X-ray detectors generally consist of large-area active matrix arrays combined with X-ray sensitive materials, such as thallium-doped cesium-iodide (CsI:Tl).[1,2] Advantages of such detectors over X-ray film include the immediate availability of the acquired images for inspection on a monitor and the reusability of the detector. Moreover, compared to storage phosphor systems (SPS),[1,3] a-Si flat-panel detectors are also applicable to real-time acquisition of moving X-ray images, such as fluoroscopy and cine-angiography. At the same time, a flat-panel detector is smaller and of less weight than an image-intensifier/CCD-detector front end used traditionally in fluoroscopy. Limitations in today's technology of fabricating large-area active matrix arrays, however, result in a certain, very low percentage of the pixels to be inactive. Inactive pixels may occur alone, or in clusters of, e.g., one or several adjacent lines (see e.g. Ref. 2, p. 287). The missing information at such inactive pixel sites needs to be corrected by interpolation. In static radiographs, defect interpolation can only be carried out by intraframe filtering. To prevent unacceptable blurring of the interpolated data, non-linear interpolation methods like median filtering or directional interpolation[4] are often used. An alternative to spatial-domain

processing, in particular for larger defects, is our spectral-domain approach described in Ref. 5, where defect interpolation is approached as the FFT-based local deconvolution of the spectrum of the defect window from the observed image spectrum. Practically, the deconvolution is solved by successive approximation.[6, 7] This approach is also used for spatial concealment of missing blocks in error-prone communication environments.[8]

In fluoroscopy or cine-angiography, interpolation can be extended to spatiotemporal approaches. Unlike pure intraframe interpolation, a motion compensated interframe algorithm may attempt to truly recover the missing information by tracking it in previous frames. Motion estimation is hence an integral part of our concept. A spatiotemporal approach towards recovery of missing data was already applied to restoration of archived, degraded film material.[9] Unlike in the restoration of degraded film material, where the defect locations are random and moving, we may here consider the defects as static over reasonable time intervals, and as known from an initial calibration step. An important point then is to ensure that the motion estimation algorithm is not misled by the static defects.

In the following, we first describe our motion estimator, which starts with block matching. Since the estimation of motion is an ill-posed problem,[10] and robustness to noise is of particular relevance for motion estimation in X-ray fluoroscopy with its low signal-to-quantum noise ratio,[1] the block matching procedure is followed by a computationally efficient regularization step[11] (cf. also Ref. 12). The block matching procedure itself is sped up by successive elimination,[13, 14] and an efficient implementation of the error measure calulation. Further speedup is possible by multiscale processing. Moreover, if motion estimation is to be used for defect interpolation only, considerable computational savings are obtained by confining it to areas around the inactive lines.

We then discuss three methods of spatiotemporal interpolation in the motion-compensated data, viz. direct filling-in by the motion compensated predecessor, spatiotemporal multilevel median filtering and weighted spatiotemporal averaging. The concept is tested on routine clinical fluoroscopy sequences with simulated defects of up to six adjacent missing lines.

2. MOTION ESTIMATION

2.1. Motion Estimation by Constrained Optimization

We estimate motion by minimizing a criterion which considers both the observed image data and prior expectations about spatial and temporal smoothness of the estimated motion fields.[11, 14] Since X-ray image sequences often contain abrupt and fast motion, we opted for a block matching algorithm rather than for gradient-based approaches ("optical flow"), which rely on quasi-continuous differentiable sequences.

The data term considers the squared or absolute pixelwise differences between two successive images $G_t = \{g_t(k)\}$ and $G_{t-1} = \{g_{t-1}(k)\}$, $k \in \Pi$, where t and $t-1$ are successive frame indices, k is a pixel coordinate, and $g_t(k)$ denotes the gray level in G_t at pixel k. Π denotes the image plane. For a motion field $V_t = \{v_t(k)\}$, $k \in \Pi$, from frame G_t to G_{t-1}, the MSE is then given by

$$E_D(V_t) = \sum_{k \in \Pi} (g_t(k) - g_{t-1}(k + v_t(k)))^2 \tag{1}$$

Here, $v_t(k)$ is the motion vector pointing from pixel k in G_t to pixel $k + v_t(k)$ in G_{t-1}. Alternatively, one might consider the mean absolute error (MAD)

$$E_D(V_t) = \sum_{k \in \Pi} |g_t(k) - g_{t-1}(k + v_t(k))| \tag{2}$$

In both definitions, we have dropped the normalization by the number $|\Pi|$ of pixels in each image. These measures are widely used in motion analysis of image sequences.

The MSE as defined above implicitly assumes the remaining noise in the motion-compensated difference images to be independent and identically Gaussian distributed, while the MAD assumes a Laplacian distribution. In quantum-limited X-ray imaging, the dominant noise source is, however, X-ray quantum noise which obeys

a Poisson distribution.[1] For realistic quantum counts, the Poisson distribution may be approximated by a Gaussian one with signal-dependent variance (see Appendix in Ref. 11). The variance at pixel k is thus originally proportional to the mean signal value at site k. This linear relationship is modified by later nonlinear conversion stages, such as "white compression". The dependence of the variance on the signal mean can be calibrated for given parameter settings, and stored in a look-up table (see, e.g., Refs. 1, 11, 15). At each pixel k, the appropriate variance estimate $\sigma^2(k)$ can then be determined by first calculating the gray level average in a local neighbourhood, and then retrieving the corresponding variance estimate from the look-up table. In the MSE criterion, the thus approximated Poisson model leads to a normalization by the spatially varying variance according to

$$E_{POISS}(V_t) = \sum_{k \in \Pi} \frac{(g_t(k) - g_{t-1}(k + v_t(k)))^2}{\sigma^2(k)} \tag{3}$$

Spatial smoothness is assessed by the differences of neighbouring motion vectors. With N_k denoting the 3×3-neighbourhood around pixel k, the spatial smoothness "error" of the motion field V_t is defined as

$$E_s(V_t) = \lambda_s \sum_{k \in \Pi} \sum_{l \in N_k} ||v_t(k) - v_t(l)||_2^p \tag{4}$$

where λ_s is a regularization parameter. The exponent p may be set between 1 and 2, and allows to control the occurrence of motion edges without having to specify a threshold: $p = 2$ assumes a Gauss-Markov random field model for the motion fields (cf. for image restoration Ref. 16), which heavily penalizes large differences between adjacent motion vectors. Varying p implicitly assumes a Generalized Gauss-Markov model. As p approaches one, the underlying distribution approaches a Laplacian distribution. The tails of this distribution are much larger than those of the Gaussian one, thus making larger differences between adjacent vectors more likely, or, in other words, imposing lower penalty on large differences than the Gaussian model does. Experiments have shown that $p = 1.3$ yields smooth motion fields with well-preserved motion boundaries.[11]

Finally, we define a similar term for assessing temporal smoothness between two successive motion fields V_t and V_{t-1} as

$$E_t(V_t) = \lambda_t \sum_{k \in \Pi} ||v_t(k) - v_{t-1}(k)||_2^p \tag{5}$$

The total energy to be minimized by estimation of V_t is then given by

$$C(V_t) = E_{POISS} + E_s + E_t \tag{6}$$

Minimization of this criterion by appropriately finding the motion field V_t can be regarded as finding the maximum a posteriori (MAP) estimate of the motion field,[11, 17] where the prior expectations on the sought motion fields are modelled by a Generalized Gauss-Markov random field within the image plane, and by a Markov chain along the temporal axis. The remaining noise in the motion-compensated difference images is characterized by the above approximation to the Poisson model.

The estimate V_t is determined by a deterministic relaxation of the ICM-type.[18] The relaxation is initialized by block matching with non-overlapping blocks, with a typical block size of 16×16 pixels for 512×512-pixel images. The resulting, generally very noisy motion field is then optimized subject to the criterion (6) by considering each motion vector $v(k)$, and substituting for it on a trial basis each of the following candidate vectors:

- each of its neighbours in N_k

- its temporal predecessor

- the four vectors differing from $v(k)$ by a half-pel

- the average of the vectors in N_k

For each of these candidate vectors, the optimization criterion $C(V_t)$ is recalculated. Since only vectors from a small spatiotemporal neighbourhood are involved, this recalculation can be done locally. Finally, the candidate which minimizes $C(V_t)$ is kept before moving to the next motion vector.

To save computation efforts, this optimization is carried out for one motion vector per block only, i.e. the blocks are considered as macro-pixels. These vectors are assigned to the center of each block. Between these vectors, linear interpolation is finally applied. This relaxation converges in no more than three iterations to a smooth local optimum.

2.2. Defect Blanking

For motion-compensated defect replenishment, it suffices to apply the motion estimator only to the defects and their direct surroundings. If the found motion vectors shall also be used for later processing tasks, such as noise reduction by motion compensated temporal filtering,[11, 19] moving object analysis or for MPEG-like hybrid data compression purposes, it is required that motion be estimated over the entire image plane Π. In both cases, however, motion estimation around the inactive pixels may fail if the block matcher locks on to the temporally static defects. Therefore, the defects are cut out of each block during error measure calculation. An alternative would be to first interpolate the missing data provisionally by an intraframe algorithm in order to estimate motion. The defect blanking aproach, however, is independent of the performance of the provisional interpolation algorithm.

2.3. Motion Estimation with Increased Computation Efficiency

Clearly, the main computational effort of this motion estimator rests with block matching, which requires a full search over a reasonably large search area. Several ways exist which permit a substantial reduction of this computational load. First, one may stop evaluation of the MSE or MAD criterion for a new candidate vector once the current minimum is reached during summing over the block-internal squared or absolute differences. Since the testing condition implies some overhead, a good compromise is to test after each line of a block, and to stop summing and switch to the next search position if the current minimum is reached. Secondly, one may use inequality relations between the arithmetic and square means to eliminate unnecessary computations of the matching criterion. At each new search position, the difference between the arithmetic block mean values normalized by the number of block-internal pixels is evaluated first. The MSE needs to be evaluated only if this normalized difference is smaller than the current minimum.[13, 20] Generally, the computational effort saved by the thus eliminated search positions outweighs by far the moderate overhead for calculation of the block mean values. A further speedup is possible by dividing the blocks into subblocks, which allows a tighter assessment of whether or not a search position can be eliminated from further consideration.[14, 20]

3. DEFECT REPLENISHMENT

3.1. Motion-Compensated Predecessor

Defect interpolation by using the motion-compensated predecessor (MCP) assumes that the information missing in frame G_t is, due to motion, available at other, active locations in the previous frame G_{t-1}. After motion estimation, these locations in frame G_{t-1} are known, so that the defects in G_{t-1} can directly be filled. While straightforward and intuitive, this approach has two drawbacks: first, it is assumed that the missing information is indeed visible in G_{t-1}. Evidently, if the estimated motion vector points to a defect in G_{t-1}, this assumption is violated. This includes the case of zero motion, where the motion vector points to the same defect in the previous frame. To solve this problem, one could either try to trace motion over several previous frames until the sought information is found, or by switching to a spatial interpolation procedure. The second drawback of this approach is that, due to the absence of any filtering, it does not safeguard against motion estimation errors.

3.2. Spatiotemporal Median Filtering

Both of the above drawbacks of MCP may be adressed by spatiotemporal filtering of the motion compensated image data. First, the spatiotemporal support of a filter implies that in case temporal interpolation is not possible, spatial information is still available. On the other hand, using a suitable nonlinear filter also implies that the interpolation will to a certain degree be robust with respect to motion estimation errors. We here use the spatiotemporal two-level median filter described in Ref. 9 for film restoration. The filter anatomy is as follows: In a first stage, the median y_i, $i = 1, \ldots, 5$ is calculated for each of the five spatiotemporal neighbourhoods W_i in Fig. 1. Each of these neighbourhoods extends over the current, previous and next frames. Two of the neighbourhoods, viz. W_1 and W_2 are defined such that they cover only a minimal area (one pixel) in the current frame, and larger, directional areas in the past and next frame. Vice versa, the windows W_3 and W_4 cover a large area in the current frame, while the window W_5 treats all three frames equally. The second filter stage then determines the filter output as the median over the five window-internal medians y_i (Fig. 2). In the presence of motion vectors pointing to non-defective areas in the motion compensated past and next frame, this filter will provide reasonable interpolation results even for large defects via windows W_1, W_2 and W_5. In case no motion is present (or if the motion vectors point to other inactive pixels in the past and next frame), the filter will still provide an interpolation result if the extent of the inactive area is small compared to the spatial window size.
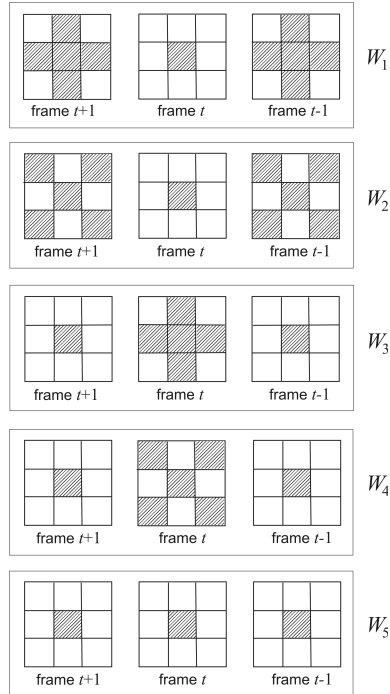

Figure 1: Spatiotemporal support windows of the two-stage median filter.

3.3. Motion Compensated Spatiotemporal Weighted Averaging

This method starts by formulating defect interpolation as a least-squares problem. A missing intensity value is sought such that it minimizes the variance among its motion compensated neighbours in space and time. Thus, the interpolation result $x_t(m)$ at an inactive pixel m in frame G_t is sought such that

$$C(x_t(m)) = \sum_{i \in N_t} (g_t(i) - x_t(m))^2 + \lambda \sum_{i \in N_{t-1}} (g_{t-1}(i) - x_t(m))^2 \tag{7}$$

is minimized. Here, N_t and N_{t-1} define neighbourhoods in the current and previous frame, respectively. The size of the neighbourhoods may be chosen depending on the defect size. Also, only active pixels within the
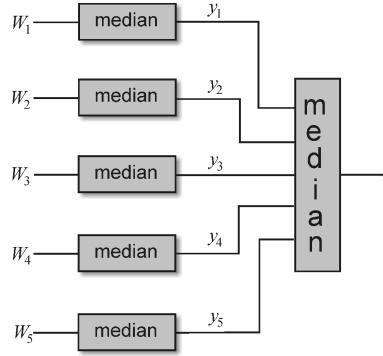
Figure 2: Diagram of the two-stage median filter.

neighbourhoods are considered in the evaluation of C. For our experiments, the neighbourhood N_t consisted of the eight nearest pixels to m. The neighbourhood N_{t-1} comprised the motion compensated predecessor $m + v_t(m)$ and its four horizontally or vertically adjacent pixels. The parameter λ permits to adjust the balance between spatial and temporal information. The solution $x_t(m)$ then is the weighted spatiotemporal average

$$x_t(m) = \frac{\sum_{i \in N_t} g_t(i) + \lambda \sum_{i \in N_{t-1}} g_{t-1}(i)}{|N_t| + \lambda |N_{t-1}|} \tag{8}$$

4. RESULTS

4.1. Image Material

We tested our algorithms with two fluoroscopy sequences recorded in clinical routine. The sequences were acquired with an image intensifier/camera chain, and were thus originally defect-free. Into these sequences, we simulated inactive areas. Fig. 3 shows one frame taken from the first sequence. The frame size is 512×512 pixels. The data are rather noisy. The sequence exhibits little global motion. Only the vertically orientated instrument visible in the upper right quadrant of the image plane moves swiftly in horizontal direction across the inactive columns. To this sequence two artificial inactive regions were added: a three-pixel wide row starting with row number 254, and a three-pixel wide column starting at column 364.

The second sequence shows intestines with considerable global, mainly upward motion (Fig. 4). In this sequence defects were simulated as a three-pixel wide row starting with row 149, and a six-pixel wide row starting in row 349.

In both sequences, motion was estimated with blocks of size 16×16 pixels, $p = 1.3$, $\lambda_t = \lambda_s = 2$.

4.2. Motion-Compensated Predecessor

This method yields good results for regions with clearly expressed motion, where the missing information is indeed available in previous frames. This is evident from Fig. 5: Good interpolation is achieved over the moving objects, whereas no interpolation is possible in the static areas, where the defects remain visible unless filled by another method. In the second sequence with its global motion, this is vastly different (Fig. 6): all defects are corrected except those outside the circular acquisition window of the image intensifier. On the other hand, the zoomed region in Fig. 5 shows that, if information can be inserted into the defective area, the result looks very natural.

4.3. Two-Stage Spatiotemporal Median Filter

Fig. 7 shows the result for the motion compensated two-stage median filter. Evidently, even the defects in static regions were interpolated due to the spatiotemporal filter support. A similar result is shown for the second sequence in Fig. 8.

Figure 3. Fluoroscopy sequence frame with simulated defective lines and columns. For better visibility, the defects are represented with maximum gray level.The rectangle indicates a region for which enlarged results are shown later on.
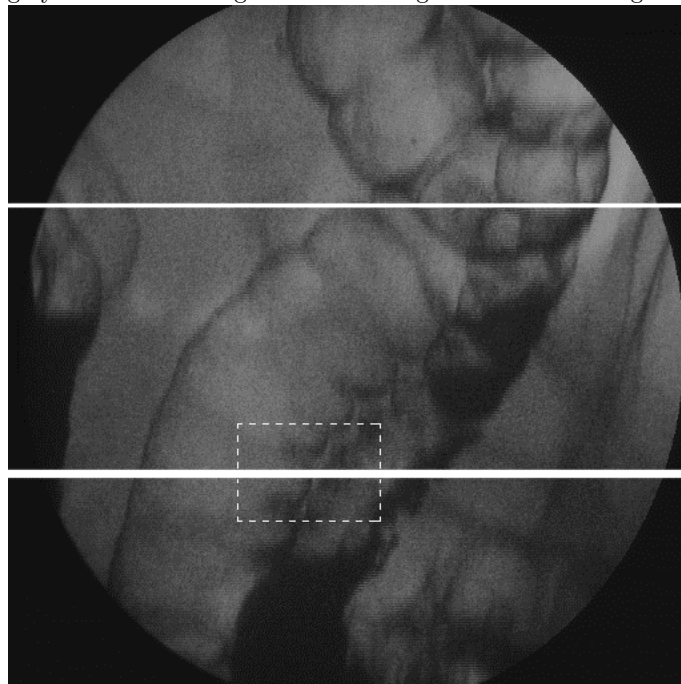

Figure 4. Fluoroscopy sequence frame with simulated defective lines. The rectangle indicates a region for which enlarged results are shown later on.

4.4. Spatiotemporal Weighted Averaging

Like the two-stage median filter, this method makes use of a spatiotemporal neighbourhood, thus mitigating or even eliminating problems caused by low or no motion. Fig. 9 shows the result for the first sequence, and Fig.
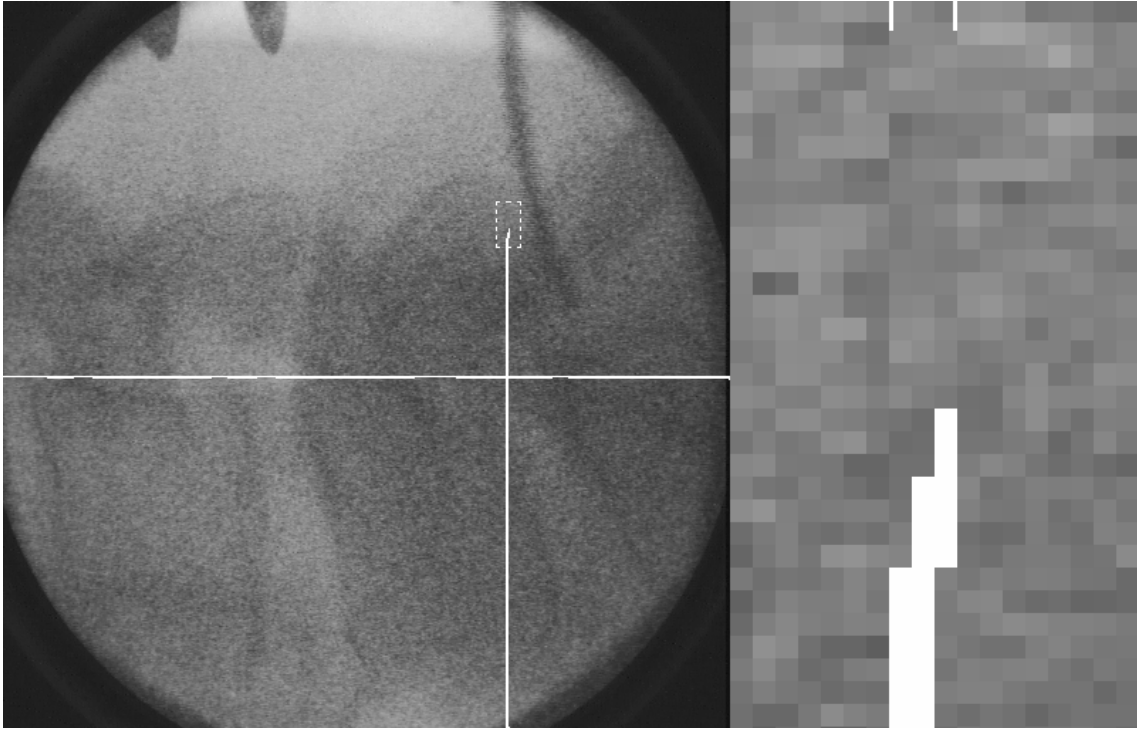
Figure 5. Results obtained for the first sequence by the MCP method. The zoomed section on the right is indicated by a rectangle in the image on the left.
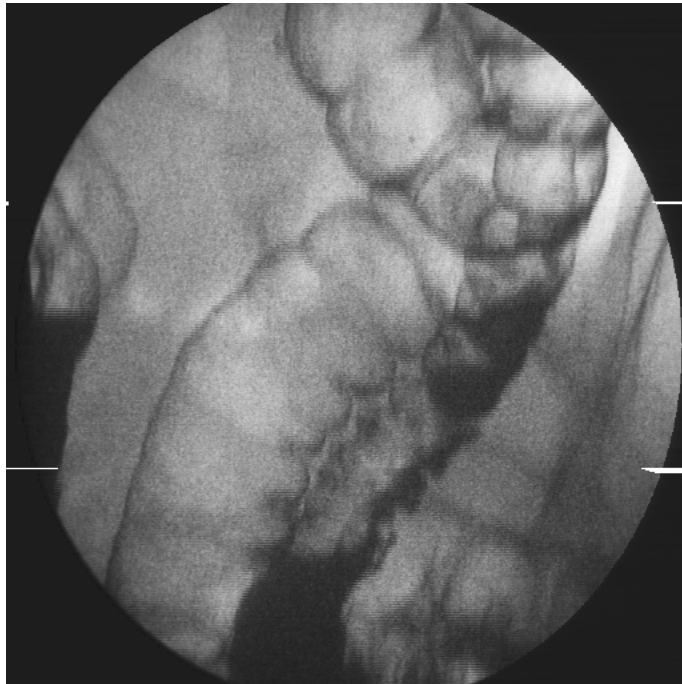
Figure 6: MCP interpolation result for the second sequence.

10 for the second one.
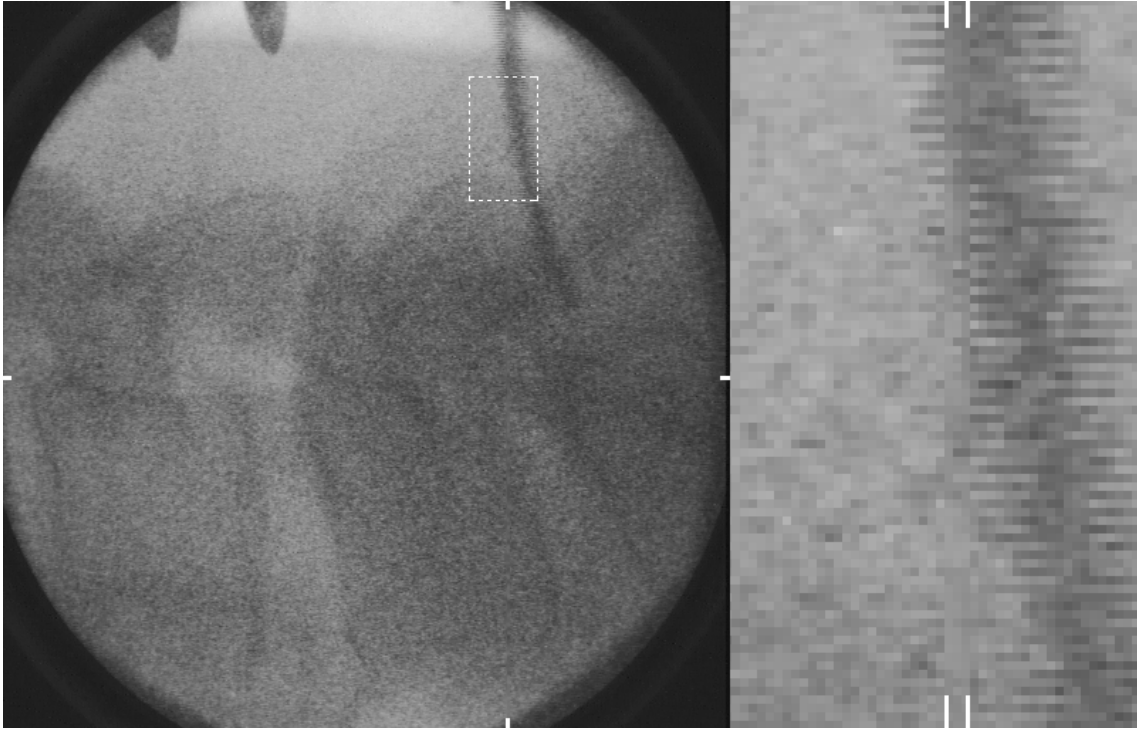
Figure 7. Interpolation result obtained by the multilevel median filter, with the region indicated by the recangle enlarged on the right-hand side. The original position of the defect is marked by the white bars.

Figure 8: Interpolation result obtained by the multilevel median filter.

Finally, for a direct comparison of the three approaches, Fig. 11 shows a strongly zoomed version of the

Figure 9: Interpolation result obtained by weighted spatiotemporal averaging.
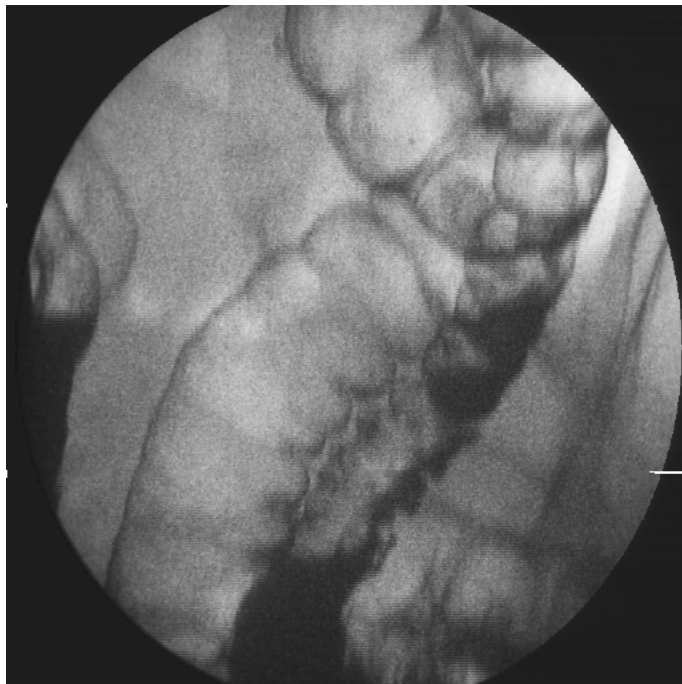
Figure 10: Interpolation result obtained by weighted spatiotemporal averaging.

region indicated by the rectangle in the second sequence, which is placed over the six-pixel wide defect. All three methods provide reasonable interpolation results due to the presence of strong motion. As expected, the weighted averaging filter introduces the strongest blur.

Figure 11. Zoomed version of the interpolation results for the region indicated by the rectangle in Fig. 4. Left: MCP, middle: multilevel median, right: weighted average.

5. CONCLUSIONS

As a spatiotemporal extension to our earlier purely spatial approaches,[5] we have described defect interpolation algorithms for moving X-ray image acquisition by flat-panel detectors. The algorithms require motion estimation and compensation, where the motion estimation procedure is made blind to the static defects. In principle, motion estimation could be limited to the vicinities of the known defect areas. In view of potential later processing stages, which might also need motion information, it appears reasonable to estimate motion over the entire image plane, and reuse the motion field for, e.g., temporal noise reduction, image analysis or data compression. The interpolation itself is carried out by either direct insertion of the temporal predecessor in motion direction, or by a spatiotemporally filtered value. The latter has the advantage of also being applicable in the absence of motion, and of being more robust against motion estimation errors. The nonlinear multilevel median filter caused least blur in the interpolated data. It appears therefore as the method of choice, and is applicable to probably all defects occurring in practice. In the very unlikely case of a defect being too large to be interpolated by the multilevel median filter, an intraframe interpolation algorithm (e.g., Ref. 5) can be used as a fallback.

REFERENCES

1. T. Aach, U. Schiebel, and G. Spekowius, "Digital image acquisition and processing in medical x-ray imaging," *Journal of Electronic Imaging* **8**(Special Section on Biomedical Image Representation), pp. 7–22, 1999.
2. J. A. Rowlands and J. Yorkston, "Flat panel detectors for digital radiography," in *Handbook of Medical Imaging*, J. Beutel, H. L. Kundel, and R. L. van Metter, eds., pp. 223–328, Springer Verlag, 2000.
3. W. Hillen, U. Schiebel, and T. Zaengel, "Imaging performance of a digital storage phosphor system," *Medical Physics* **14**(5), pp. 744–751, 1987.
4. F. Xu, H. Liu, G. Wang, and B. A. Alford, "Comparison of adaptive linear interpolation and conventional linear interpolation for digital radiography systems," *Journal of Electronic Imaging* **9**(1), pp. 22–31, 2000.
5. T. Aach and V. Metzler, "Defect interpolation in digital radiography - how object-oriented transform coding helps," in *Medical Imaging 2001*, M. Sonka and K. M. Hanson, eds., pp. 824–835, SPIE Vol. 4322, (San Diego, USA), February 17–22 2001.
6. A. Kaup and T. Aach, "Coding of segmented images using shape-independent basis functions," *IEEE Transactions on Image Processing* **7**(7), pp. 937–947, 1998.
7. R. Sottek, K. Illgner, and T. Aach, "An efficient approach to extrapolation and spectral analysis of discrete signals," in *Informatik Fachberichte 253*, W. Ameling, ed., pp. 103–108, ASST 90, Springer Verlag, (Aachen, FRG), September 1990.
8. K. Meisinger and A. Kaup, "Örtliche Fehlerverschleierung von gestört empfangenen Bilddaten durch frequenzselektive Extrapolation," in *Elektronische Medien: 10. Dortmunder Fernsehseminar*, pp. 189–194, ITG Fachbericht 179, (Dortmund), September 2003.
9. A. K. Kokaram, R. D. Morris, W. J. Fitzgerald, and P. J. W. Rayner, "Interpolation of missing data in image sequences," *IEEE Transactions on Image Processing* **4**, pp. 1509–1519, 1995.

10. M. A. Bertero, T. Poggio, and V. Torre, "Ill-posed problems in early vision," *Proceedings of the IEEE* **76**(8), pp. 869–889, 1988.

11. T. Aach and D. Kunz, "Bayesian motion estimation for temporally recursive noise reduction in x-ray fluoroscopy," *Philips Journal of Research* **51**(2), pp. 231–251, 1998.

12. C. Stiller, "Motion estimation for coding of moving video at 8kb/s with Gibbs modeled vector field smoothing," in *Proceedings Visual Communications and Image Processing 90*, M. Kunt, ed., **1360**, pp. 468–476, SPIE, (Lausanne, Switzerland), October 1990.

13. W. Li and E. Salari, "Successive elimination algorithm for motion estimation," *IEEE Transactions on Image Processing* **4**(1), pp. 105–107, 1995.

14. C. Mayntz, T. Aach, and G. Schmitz, "Acceleration and evaluation of block-based motion estimation for x-ray fluoroscopy," in *Medical Imaging 2001*, M. Sonka and K. M. Hanson, eds., pp. 1075–1083, SPIE Vol. 4322, (San Diego, USA), February 17–22 2001.

15. T. Aach and D. Kunz, "Spectral estimation filters for noise reduction in x-ray fluoroscopy imaging," in *Proceedings EUSIPCO-96*, G. Ramponi, G. L. Sicuranza, S. Carrato, and S. Marsi, eds., pp. 571–574, Edizioni LINT Trieste, (Trieste, Italy), September 10–13 1996.

16. C. Bouman and K. Sauer, "A generalized Gaussian image model for edge-preserving MAP-estimation," *IEEE Transactions on Image Processing* **2**(3), pp. 296–310, 1993.

17. T. Aach and D. Kunz, "Robust motion vector relaxation for x-ray fluoroscopy using generalized Gauss-Markov random fields," in *Proceedings Aachener Workshop: Bildverarbeitung in der Medizin 1998: Algorithmen, Systeme, Anwendungen*, T. Lehmann, V. Metzler, K. Spitzer, and T. Tolxdorff, eds., pp. 19–23, Springer Verlag (Informatik aktuell) ISBN: 3-540-63885-7, (Aachen), March 26 - 27 1998.

18. J. Besag, "On the statistical analysis of dirty pictures," *Journal Royal Statistical Society B* **48**(3), pp. 259–302, 1986.

19. E. Dubois and S. Sabri, "Noise reduction in image sequences using motion compensated temporal filtering," *IEEE Transactions on Communications* **32**(7), pp. 826–831, 1984.

20. M. Brünig and W. Niehsen, "Ein Algorithmus zur schnellen Bewegungsschätzung in Bildfolgen," in *Proceedings ITG-Fachtagung Codierung für Quelle, Kanal und Übertragung*, **146**, pp. 53–58, (Aachen), March 1998.